
SUPERVISED LEARNING FOR MULTI ZONE SOUND FIELD REPRODUCTION UNDER HARSH ENVIRONMENTAL CONDITIONS

A PREPRINT

Henry Sallandt*

Institute of Fluid Mechanics and Engineering Acoustics
Technical University Berlin
Müller-Breslau-Str. 15, 10623 Berlin, Germany
jannick.h.sallandt@tu-berlin.de

Philipp Krah

Institute of Mathematics
Technical University Berlin
Straße des 17. Juni 136, 10623 Berlin, Germany
krah@math.tu-berlin.de

Mathias Lemke

Institute of Fluid Mechanics and Engineering Acoustics
Technical University Berlin
Müller-Breslau-Str. 15, 10623 Berlin, Germany
mathias.lemke@tnt.tu-berlin.de

December 15, 2021

ABSTRACT

This manuscript presents an approach for multi zone sound field reproduction using supervised learning. Traditional multi zone sound field reproduction methods assume constant speed of sound, neglecting nonlinear effects like wind and temperature stratification. We show how to overcome these restrictions using supervised learning of transfer functions. The quality of the solution is measured by the acoustic contrast and the reproduction error. Our results show that for the chosen setup, even with relatively small wind speeds, the acoustic contrast and reproduction error can be improved by up to 16 dB, when wind is considered in the trained model.

Keywords sound field reproduction · supervised learning · acoustic transfer function · Euler equations · physics informed machine learning

1 Introduction

Supervised learning is a field in machine learning where possibly complicated dependencies between chosen inputs and outputs are not analytically solved but learned by e.g. neural networks that try to approximate the relevant correlation. Neural networks are used in various acoustic applications such as speech recognition [19], characterisation of reverbing rooms [5], echo cancellation [11] and various others [2].

Sound field reproduction is aimed to create different sound experiences for listeners at different locations. There are several ways to perform sound field reproduction such as wave field synthesis [3] or lower/higher order ambisonics [7, 20]. Usually nonlinear effects such as wind and temperature stratification are

neglected, which can lead to errors whose relative sizes are dependent on the application. In addition to these studies there are also pressure matching methodologies [4, 15, 6, 9] which are based on the acoustic transfer function and traditionally use the same neglect of wind and temperature stratification.

Another method for sound field reproduction is the adjoint approach [13, 16]. Although it copes with nonlinear effects like wind and temperature, it comes with high computational costs because it is based on solving the full set of compressible Euler equations. Furthermore, the optimisation can be trapped in local minima and setting it up for systems with complicated boundary conditions and geometries can be difficult.

Here, we propose an alternative strategy based on the multi zone sound field reproduction algorithm of [6], which makes use of the acoustic transfer function, but incorporates nonlinear effects. The acoustic transfer function describes how sound propagates between a speaker and a microphone. When generalising the concept to nonlinear acoustics, the transfer function can still be useful although hard to be analytically determined. Here, we make use of supervised learning, to capture nonlinear effects like wind and temperature stratification. Instead of training the neural network directly on the acoustic transfer function, we use the knowledge of sound propagation. By combining the physical information, the structure of the transfer function, with neural networks we simplify the functions that have to be approximated by the networks and makes our approach interpretable.

The manuscript is organised as follows: Section 2 introduces the methodology. Section 2.1 defines the acoustic transfer function and the generalisations made for supervised learning. Furthermore we summarise the methodology of [6] in section 2.3 and give insights into our optimisation and training procedure (see Sections 2.2 and 2.4). Finally, in Section 3 the methodology is applied to different analytical and numerical test cases. In Section 3.1 we reproduce the results from [6] and validate the proposed methodology. Thereafter, the setup is generalised to applications where wind is considered in Section 3.2. Here, a uniform wind flow is introduced to have an analytical solution for validation and reproducible results. The effects of the training data's sample density on the results are examined. Lastly, the value of the methodology is shown in Section 3.3 in a setup where no analytical solution is known with a logarithmic wind profile and a temperature gradient. We finish with a discussion in Section 4 where we recap the results and give a short outlook.

2 Methodology

In this section we introduce the acoustic transfer function, its generalised form and how it can be learned from data. Furthermore, we show how the learned transfer function can be used inside the multizone sound field reproduction method of [6] to include nonlinear effects.

2.1 Recreation of the Acoustic Transfer Function

The acoustic transfer function $g_{nm} \in \mathbb{C}$ relates a measured sound signal, i.e. pressure p_n at position $\mathbf{x}_n \in \mathbb{R}^3$ (microphone) to its sound source w_m at $\mathbf{x}_m \in \mathbb{R}^3$ (speaker):

$$p_n(t) = \sum_m g_{nm} w_m(t). \quad (1)$$

It can be expressed as follows:

$$g_{nm} = \tilde{a}_{nm} \exp(i\varphi_{nm}), \quad \varphi_{nm} = \tilde{\varphi}_{nm} + k\|\mathbf{x}_n - \mathbf{x}_m\|. \quad (2)$$

Here, \tilde{a}_{nm} is a function modulating the amplitude, k the wavenumber, φ_{nm} the phase shift and $\tilde{\varphi}_{nm}$ the phase modulation. Apart from the phase shift caused by the wave having to travel a physical distance $s_{nm} = \|\mathbf{x}_n - \mathbf{x}_m\|$, we consider the phase modulation to contain several kinds of possibly nonlinear effects, like dispersion. Given that we neglect wind for now, the amplitude modulation can be dependent on the frequency of the speaker (e.g. if the source is not a point source but a Gaussian source

[17]) and the phase modulation can also be dependent on the frequency.

The consideration of wind leads to more complicated acoustic transfer functions. Since wind stretches and compresses sound waves, it is useful to introduce the wave number modulation factor $\tilde{k}_{nm}(Ma)$ into Equation (2) which is dependent on the ratio between wind speed and speed of sound c , known as the Mach number Ma . The wind also leads to an in- or decrease in amplitude and influences the phase shift. Therefore $\tilde{a}_{nm}(f, Ma)$ and $\tilde{\varphi}_{nm}(f, Ma)$ are dependent on the Mach number.

The acoustic transfer function $g_{nm}(f, Ma): \mathbb{R}^2 \rightarrow \mathbb{C}$ can be thus expressed as a function of the frequency and Mach number

$$g_{nm}(f, Ma) = \tilde{a}_{nm}(f, Ma) \cdot \exp\left(i\left(\tilde{\varphi}_{nm}(f, Ma) + \tilde{k}_{nm}(Ma)ks_{nm}\right)\right), \quad (3)$$

where the nonlinear functions $\tilde{a}_{nm}(f, Ma)$, $\tilde{\varphi}_{nm}(f, Ma)$ and $\tilde{k}_{nm}(Ma)$ need to be determined from data or measurements. Since nonlinear effects can vary between different spatial positions, the three functions are dependent on the locations \mathbf{x}_n and \mathbf{x}_m . Hence, in this manuscript we use separate neural networks to approximate \tilde{a}_{nm} , $\tilde{\varphi}_{nm}$ and \tilde{k}_{nm} . As an alternative approach, the neural network could be used for all speaker and microphone combinations. However, this would lead to an even more complex function to be approximated, with poor approximation quality and less insight into the system.

Note, that the functions have at most two inputs and are thus low-dimensional. In this case, another possibility would be to interpolate between the measured values. This is not done here, since it would pose the assumption, that the outputs have to be a smooth function of the inputs, which doesn't have to be the case for complicated systems.

2.2 Training Procedure

Finally, we introduce the generalised acoustic transfer function $\mathbf{G}^{\text{NN}} = (g_{nm}^{\text{NN}})_{m=1\dots M, n=1\dots N}$ between microphone at \mathbf{x}_n and speaker at \mathbf{x}_m :

$$g_{nm}^{\text{NN}}(f, Ma) = \tilde{a}_{nm}^{\text{NN}}(f, Ma) \cdot \exp\left(i\left(\tilde{\varphi}_{nm}^{\text{NN}}(f, Ma) + \tilde{k}_{nm}^{\text{NN}}(Ma)ks_{nm}\right)\right). \quad (4)$$

As explained above, \mathbf{G}^{NN} is able to include nonlinear effects using the learnable functions $\tilde{a}_{nm}^{\text{NN}}(f, Ma)$, $\tilde{\varphi}_{nm}^{\text{NN}}(f, Ma)$ and $\tilde{k}_{nm}^{\text{NN}}(Ma)$, which are approximated by fully connected neural networks, as indicated by the NN in their superscript.

Note, that the neural networks get Ma as single input for the wind speed, where in reality the wind is a continuous vector field. However, we assume a constant wind profile, which is scaled by the Mach number. It is important to note here that this restriction does not have to be imposed necessarily, as the neural networks can be trained on any physically meaningful wind profile. This is shown in Section 3. Moreover, the approach can be generalised for multiple inputs, describing the wind profile. One possible application could be the parametrization of the wind profile in a Fourier series, which is left open for future research.

In this paper, the networks are trained on simulation data, but the presented approach is also suitable for measured data. In the following, we describe how the training data for $\tilde{a}_{nm}^{\text{NN}}$, $\tilde{\varphi}_{nm}^{\text{NN}}$ and $\tilde{k}_{nm}^{\text{NN}}$ is collected from measurements of the pressure at the microphones. We assume a microphone/speaker setup similar to the one illustrated in Figure 1 with multiple sound sources (speakers) and measurement locations (microphone).

For a given (Ma, f) configuration, we measure the impulse-response correlation between every pair of speaker and microphone. Therefore, a mono frequent signal $w_m \in \mathbb{R}$

$$w_m(t) = \hat{w}_0 \sin(2\pi ft + \phi_0), \quad (5)$$

is produced by a single speaker at position \mathbf{x}_m . Since both, amplitude \hat{w}_0 and phase shift ϕ_0 of the speaker signal can be arbitrarily chosen, we can keep them constant for all microphone and speaker combinations. The pressure signal $p_n \in \mathbb{R}$

$$p_n(t) = \hat{p}_{nm} \sin(2\pi ft + \phi_{nm}), \quad (6)$$

is measured at microphone \mathbf{x}_n .

Amplitude and Phase Shift of the Pressure Signal [10] propose to perform a fast Fourier transformation (FFT) to retrieve an initial guess of the amplitude, phase shift and frequency of the signal and to refine the initial guess using a gradient descent method. Since the frequency is known a priori in this case, here the FFT is not required to get a good initial guess. The initial guess is retrieved by the following expression:

$$\hat{p}_{nm}^0 = \max_t (|p_n(t)|), \quad (7)$$

$$\phi_{nm}^0 = \begin{cases} \text{asin}(p_n(t=0)/\hat{p}_{nm}^0) & \text{if } \frac{\partial p_n(t=0)}{\partial t} \geq 0 \\ \text{asin}(-p_n(t=0)/\hat{p}_{nm}^0) + \pi & \text{if } \frac{\partial p_n(t=0)}{\partial t} < 0 \end{cases} \quad (8)$$

Thereafter the guess can be improved using a gradient descent method.

The training data for one speaker to microphone combination can be calculated from the amplitude \hat{p}_{nm} and phase shift ϕ_{nm} of the pressure at the microphone for all measured/simulated frequencies and wind speeds.

Amplitude Modulation We want the acoustic transfer function to be the response of the pressure at the microphones from a unit signal (amplitude of 1 and no phase shift) of the speaker. However, restraining to measuring the acoustic transfer function only using a unit signal is impractical. Therefore, the amplitude modulation is calculated as follows:

$$\tilde{a}_{nm} = \hat{p}_{nm}/w_0. \quad (9)$$

The neural network has two inputs (frequency and Mach number) and one output.

Wavenumber Modulation Factor The wavenumber modulation factor can be iteratively calculated with $\tilde{k}^{l=0} = 1$ as initial guess with the following scheme:

$$\tilde{k}_{nm}^{l+1} = \tilde{k}_{nm}^l - \gamma \frac{\partial}{\partial \tilde{k}_{nm}} \frac{1}{f^+ - f^-} \int_{f^-}^{f^+} \frac{\partial \tilde{\varphi}_{nm}^l}{\partial f} df \quad (10)$$

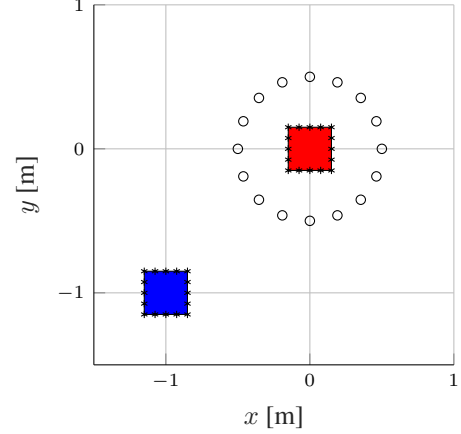


Figure 1: Simulation setup of Section 3.1. The red square is the bright zone and the blue square is the dark zone. Circles (o) are indicators for speakers, asterisks (*) for microphones.

$$\tilde{\varphi}_{nm}^{l+1} = \phi_{nm} - \phi_0 - \tilde{k}_{nm}^{l+1} k s_{nm}. \quad (11)$$

Here, f^+ is the upper limit of considered frequencies, f^- the respective lower limit and γ is a step size of the iteration process. The goal of the iteration process is that the phase modulation is constant with respect to the Mach number or, if this proves to be unfeasible for example due to dispersion, to minimise the mean of $\frac{\partial}{\partial f} \tilde{\varphi}_{nm}$.

The integral is intentionally not solved since the phase angle is brought into an interval of $[-\pi, \pi]$ and therefore it may be discontinuous (see Figure 2 and C). The numeric scheme that calculates the derivative must be able to handle this discontinuity. If the sound source is not a point source, then using the exact distance of the speaker to the microphone can lead to a wave number correction factor $\tilde{k}_{nm} \neq 1$ for $Ma = 0$. The neural network has one input (Mach number) and one output.

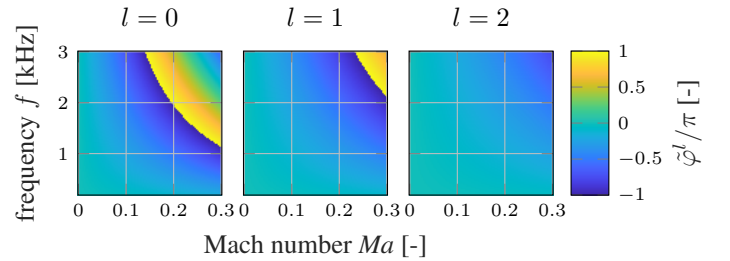


Figure 2: First iteration steps of the iteration scheme to calculate the wavenumber modulation factor of the speaker and microphone indicated by crosses in Figure 6. The initial phase modulation $\tilde{\varphi}^0$ is represented in the left colour plot ($l = 0$).

Phase Modulation The phase modulation can be calculated if the wavenumber modulation factor is known:

$$\tilde{\varphi}_{nm} = \phi_{nm} - \phi_0 - \tilde{k}_{nm} k s_{nm}. \quad (12)$$

Here, the phase shift of the speaker signal is included to achieve that the acoustic transfer function is the response of a unit

signal. To handle a possible discontinuity of the phase modulation, stemming from the periodicity of the harmonic excitation, the network is not trained on the value of the phase modulation but on $\sin(\hat{\varphi}_{nm})$ and $\cos(\hat{\varphi}_{nm})$. In order to get the phase modulation, the two dimensional arcustangens function atan2 is used (see A for detailed explanation). The neural network thus has two inputs (frequency and Mach number) and two outputs $\hat{\varphi}_{nm}^{\text{NN}} = \text{atan2}(\hat{\varphi}_{1, nm}^{\text{NN}}, \hat{\varphi}_{2, nm}^{\text{NN}})$.

Note that scaling the output to a constant interval of $[-1, 1]$ is done to ensure independence of the loss from the setup. The frequency values are scaled into the interval $[0, 1]$ to improve the performance of the neural network.

The amplitude modulation and phase modulation neural networks have two hidden layers with 15 and 10 neurons. The wave number modulation network consists of two hidden layers with 10 and 5 neurons. The activation function of all networks' hidden layers is the hyperbolic tangent sigmoid function (tansig), where the output layers do not have an activation (purelin). The neural networks are trained using MATLAB's implementation of the Levenberg-Marquardt-Algorithm (trainlm) and the training is interrupted when the mean square error loss (MSE) sinks below 10^{-7} .² The number of neurons might need to be adapted when handling more complicated cases.

2.3 Multizone Sound Field Reproduction

With the superposition principle Equation (1) and a given transfer function $\mathbf{G} = (g_{nm})_{n=1, \dots, N, m=1, \dots, M} \in \mathbb{C}^{N \times M}$ the vector of speaker signals $\mathbf{w} = (w_m)_{m=1, \dots, M} \in \mathbb{C}^M$ can be optimised towards a desired pressure $\mathbf{p}_{\text{goal}} = (p_n)_{n=1, \dots, N} \in \mathbb{C}^N$ at the microphone locations by solving the linear system³

$$\mathbf{p}_{\text{goal}} = \mathbf{G}\mathbf{w}. \quad (13)$$

For a two zone sound field reproduction problem with one dark (index d) and one bright (index b) zone, as shown in Figure 1, two optimisation problems arise [4]:

$$\min_{\mathbf{w}} \|\mathbf{p}_{\text{goal}, b} - \mathbf{G}_b \mathbf{w}\|_2^2 \quad \text{and} \quad \min_{\mathbf{w}} \|\mathbf{p}_{\text{goal}, d} - \mathbf{G}_d \mathbf{w}\|_2^2 \quad (14)$$

If the two optimisation problems are weighted equally, this leads to the following expression:

$$\begin{aligned} \mathbf{w} &= \arg \min_{\mathbf{w}} \left\| \begin{bmatrix} \mathbf{p}_{\text{goal}, b} \\ \mathbf{p}_{\text{goal}, d} \end{bmatrix} - \begin{bmatrix} \mathbf{G}_b \\ \mathbf{G}_d \end{bmatrix} \mathbf{w} \right\|_2^2 \\ &= \arg \min_{\mathbf{w}} \|\mathbf{p}_{\text{goal}} - \hat{\mathbf{G}}\mathbf{w}\|_2^2, \end{aligned} \quad (15)$$

with $\hat{\mathbf{G}} = [\mathbf{G}_b, \mathbf{G}_d]^T$.

As proposed by [18], Tikhonov regularisation is used to penalise unfeasible solutions. Therefore, we add $\lambda \|\mathbf{w}\|_2^2$, $\lambda > 0$ to the objective function J that is sought to be minimised:

$$J = \|\mathbf{p}_{\text{goal}} - \hat{\mathbf{G}}\mathbf{w}\|_2^2 + \lambda \|\mathbf{w}\|_2^2, \quad (16)$$

²see provided code at <https://github.com/henrysallandt/Supervised-Learning-for-Multi-Zone-Sound-Field-Reproduction-under-Harsh-Environmental-Conditions/>

³There are nonlinearities that affect the propagation of sound (wind, temperature stratification) but since the sound pressure amplitude is small dissipative effects can be neglected. Since the nonlinearities are fixed for all microphones and speakers the superposition principle can be assumed.

resulting in a well posed regression problem. This can be solved directly with

$$\mathbf{w} = \left[\hat{\mathbf{G}}^H \hat{\mathbf{G}} + \lambda \mathbf{I} \right]^{-1} \hat{\mathbf{G}}^H \mathbf{p}_{\text{goal}} \quad (17)$$

2.4 Optimisation Procedure

Our methodology is visualised in the flow chart shown in Figure 3. First, a frequency, a wind speed (Mach number) and the goal pressures at the microphones are chosen. Next, the neural networks are evaluated to reproduce the acoustic transfer functions using Equation (4) to generate $\hat{\mathbf{G}}$. Finally the objective function can be minimised using Equation (17). The optimisation generates a set of speaker signals w_m . This enables the reproduction of sound fields for frequencies and Mach numbers in a given parameter interval.

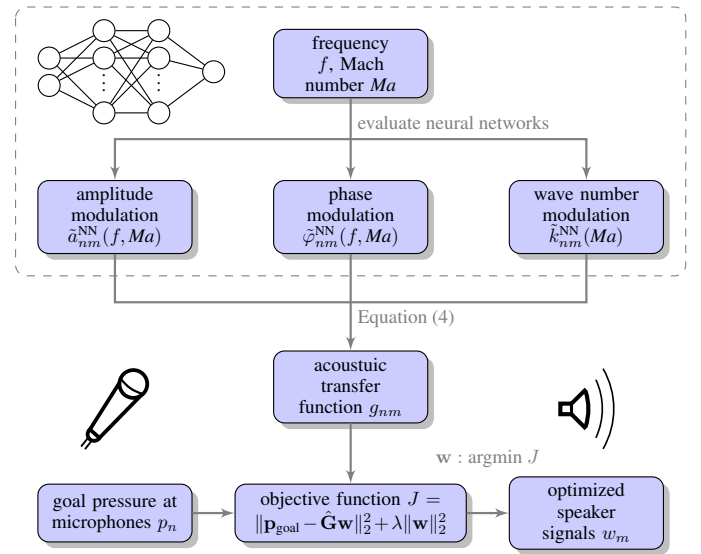


Figure 3: Flow chart of the implemented algorithm: Choose a frequency and a Mach number, evaluate the neural networks to reconstruct the acoustic transfer functions and solve the optimisation problem to get the optimised speaker signals.

3 Results

In the following section, we test the presented methodology. To compare the results, two variables are introduced: First the reproduction error (RE, lower is better) which measures the quality of the sound field in the bright zone S_b :

$$\text{RE} = 10 \log_{10} \frac{1}{|S_b|} \int_{S_b} \frac{|p_{\text{rep}} - p_{\text{goal}}|^2}{|p_{\text{rep}}|^2} dS. \quad (18)$$

Second the acoustic contrast (AC, higher is better) which measures the energy density difference between the dark zone S_d and the bright zone S_b :

$$\text{AC} = 10 \log_{10} \frac{|S_d| \int_{S_b} |p_{\text{rep}}|^2 dS}{|S_b| \int_{S_d} |p_{\text{rep}}|^2 dS}. \quad (19)$$

The regularisation introduces an additional optimisation problem which can be competing with the original optimisation problem

in Equation (15). Therefore a higher regularisation parameter λ usually leads to a lower AC and a higher RE.

3.1 Synthetic Test Case without Wind

Here, we reproduce the results of [6] to verify the proposed methodology.

Simulation Setup The simulation setup is displayed in Figure 1 and consists of a circular speaker setup with 16 uniformly spaced speakers with a radius of 0.5 m. The two sound field reproduction zones are squares with a side length of each 0.3 m placed at $(0 \text{ m}, 0 \text{ m})$ (red) and $(-1 \text{ m}, -1 \text{ m})$ (blue) with each 16 microphones on their boundaries. The red zone is the bright zone where the sound field of a monopole placed at $(5 \text{ m}, 0 \text{ m})$ is aimed to be reproduced. The blue zone is the dark zone where the pressure amplitude is aimed to be minimised. When evaluating the neural networks, the Mach number of the wind is set to zero. The speed of sound is chosen as 343 m/s.

The training data for the neural networks is created using the free field Green’s function of the 3D wave equation convoluted with a point source.⁴

Results The training of the neural networks takes approx. 1 h on a standard notebook CPU while the evaluation takes approx. 10 s and the optimisation problem is solved in a split of a second.

Figure 4 shows the RE and the AC in the frequency interval $[200, 1000]$ Hz. With the geometry shown in Figure 1 the results of the AC are equal or better than the reference results of [6] for both considered regularisation parameters and frequencies which can be seen at Figure 4a. However, Figure 4b shows that the results of [6] cannot be matched: there is some sort of a resonance at the frequency $f = 810 \text{ Hz}$ which leads to a small silent region

⁴for Green’s function of the wave equation in 3D space see B and set $Ma = 0$. For Green’s function of the wave equation in 2D space see [1] and set $Ma = 0$.

in the bright zone. The resonance is not found in [6]. This can be explained by their symmetric setup and missing noise⁵ or the Monte Carlo trials which are mentioned in [6]. The small silent region inside the bright zone can be prevented by adding a microphone in the middle of the bright zone. To better understand the behaviour of the resonance an additional setup is examined in E. Note, that we refrain from using noise in all of our test cases in order to make it deterministic and replicable for benchmarking.

A comparison of Figures 5a and 5b shows that the solution is comparable regarding the overall trend except that there is no silent region in the bright zone.

Also the AC which is shown in Figure 4a is akin for both geometries. Near the resonance, there is a slightly better AC which is due to the missing silent region in the bright zone which makes the bright zone more silent and therefore the AC lower. However, the RE, shown in Figure 4b, is much lower with the microphones in the middle of the zones and quite resistant to changes in the regularisation parameter λ . The RE is approximately 10 dB lower compared to [6].

Overall, we conclude that the proposed method and its implementation is valid for this application. For all following examples there will be a microphone placed in the middle of both zones.

3.2 Synthetic Test Case with Wind

Next, we introduce wind to the setup, an element that is abstracted from traditional sound field reproduction methods.

Simulation Setup The same simulation setup as in Section 3.1 is examined but with the introduction of uniform wind $(Ma \cdot c, 0, 0)$ m/s with c being the speed of sound. The setup is shown in Figure 6. We choose this setup, because the Green’s

⁵an examination of noise on the solution can be found in F

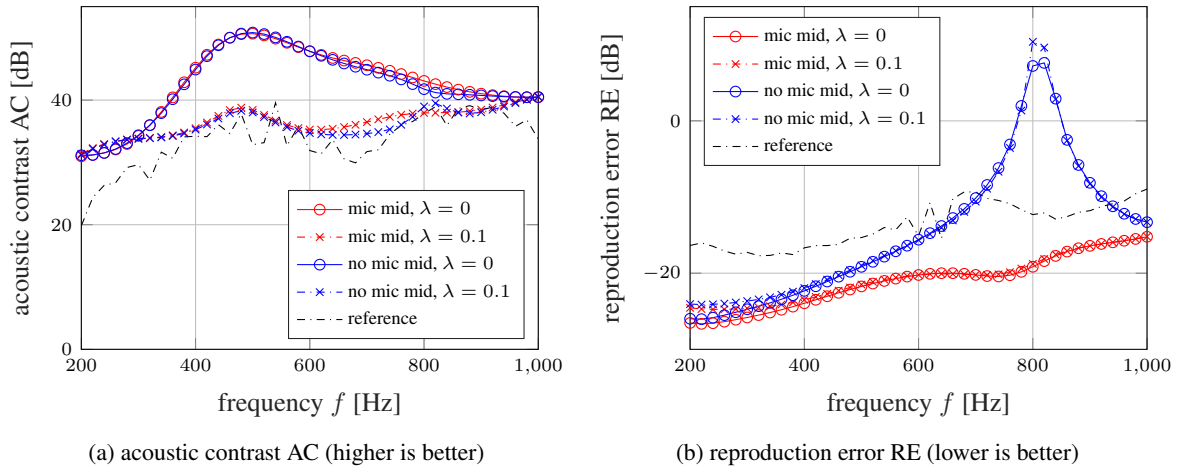


Figure 4: Comparison of the results of the solution with the microphone in the middle and without the microphone in the middle. To show the influence of the regularisation parameter the solution with two different values of the regularisation parameter is shown. For a comparison we include the results of [6].

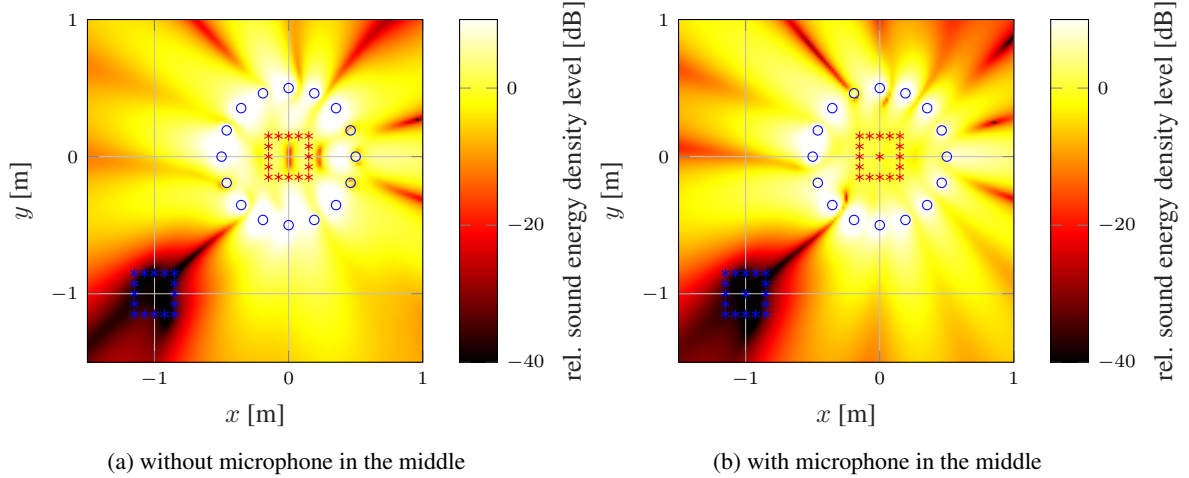


Figure 5: Comparison of the sound energy density level relative to the bright zone in dB at $f = 810$ Hz with and without microphone in the middle of the zones. Circles are indicators for speakers, asterisks for microphones.

function of the 3D wave equation is known for uniform wind⁶. Hence, this setup serves as a reproducible test case, since numerical experiments can be done easily.

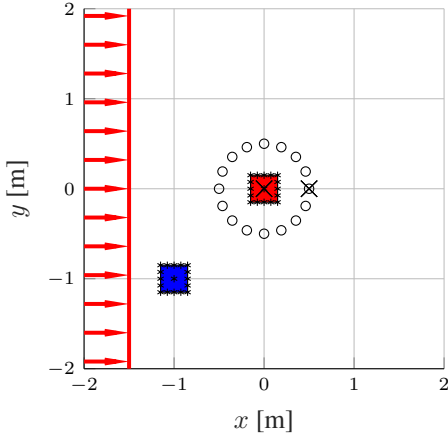


Figure 6: Geometry of the setup. The red square is the bright zone and the blue square is the dark zone. Circles are indicators for speakers, asterisks for microphones. The uniform wind profile is also shown. The two crosses are indicators for the considered microphone and speaker in Figure 7.

When training the neural network on measured data, getting a sufficient fine resolution in the frequency range is cheap. It might be costly to measure at different wind speeds and therefore the number of wind speeds is presumably relatively small. To get a feeling of how densely the training data needs to be sampled to get sufficient training data, it is initially created using 15 frequency samples and 3 wind speed samples. The samples are equidistantly distributed. Since this resolution leads to solution

⁶For Green's function of the wave equation with uniform background flow in 3D space see B. For Green's function of the wave equation with uniform background flow in 2D space see [1].

quality decreasing effects, the sampling density is increased to the point where these effects disappear (70 frequency samples, 30 wind samples).

In a next step, an investigation of the influence of the MSE loss of the neural networks on the AC and RE is performed. The MSE loss training stopping criterion of the neural networks is varied in the range $[10^{-7}, 10^{-1}]$.

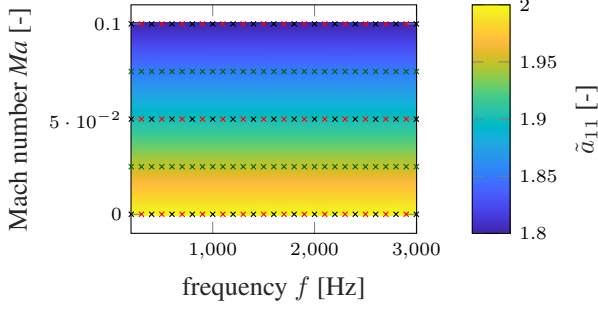
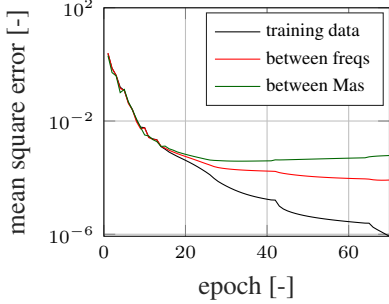
To get comparable MSE loss measurements, the trained values of the amplitude modulation and wave number modulation are scaled to the interval $[-1, 1]$. The phase modulation training data is not scaled to this interval since it is already scaled due to the sin and cos function.

Finally, the experiments are conducted using the best performing network (MSE loss stopping criterion 10^{-7}) and sufficiently dense sampled data.

Results Figure 7a shows the function of the amplitude modulation that needs to be learned by the neural networks. The functions of the phase modulation and wave number modulation are displayed in Figure 16 in D. The distribution of the training data is displayed as well. Black crosses indicate a training data point. Red and purple crosses indicate different test points. The MSE loss of the different data sets are displayed in Figure 7b. Figure 7b displays The MSE loss of the amplitude modulation network over the training epochs.

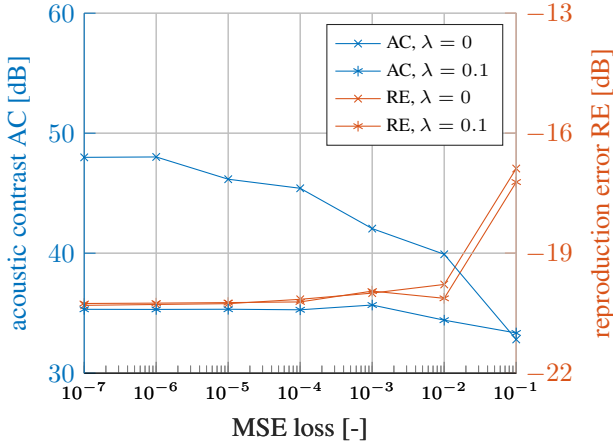
The training data MSE loss decreases down to 10^{-6} while the MSE loss of the data points in the gaps of the training data in frequency direction decreases down to 10^{-4} . Since the sampling density in wind speed direction is initially low (3 wind speeds), the MSE loss in the gaps of the training data in wind speed direction decreases only to 10^{-3} .

The influence of the MSE loss on the AC and RE is shown in Figure 8. The AC of the unregularised solution is starting to decrease at a MSE loss of 10^{-6} and continuously decreases from 48 dB down to 32.8 dB. However, a regularisation of $\lambda = 0.1$ leads to a constant AC of 35.3 dB until a MSE loss of 10^{-3} .


 (a) amplitude modulation \tilde{a}_{11} [-]


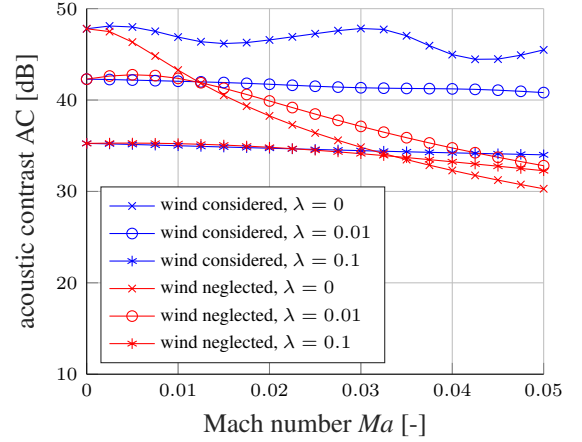
(b) Performance history of the amplitude modulation neural network with comparison of the different data sets. The data points are visualised in Figure 7a in their respective colour.

Figure 7: Influence of the sample density on the MSE loss of the amplitude modulation neural network.

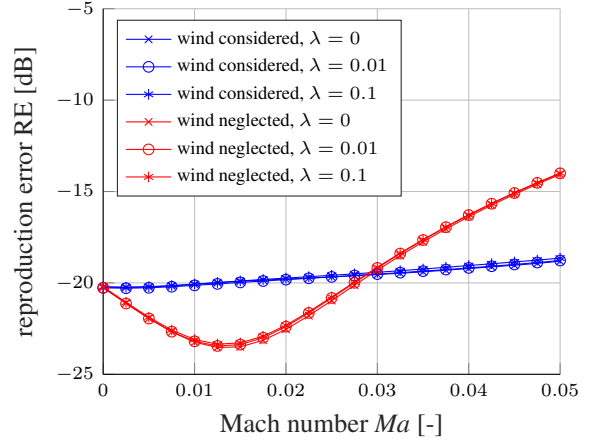

 Figure 8: Influence of the threshold MSE loss while training the neural networks on the AC and RE with $f = 600$ Hz and $Ma = 0$

While the AC decreases for rising MSE loss down to 33.4 dB, the RE is relatively resistant to changes of the MSE loss. Up to a MSE loss of 10^{-4} , the RE is constant -20.2 dB and then slowly starts increasing. At the MSE loss of 10^{-1} the RE jumps up to -17 dB.

When comparing the AC in Figure 9a for neglected and considered wind, one can see that the latter leads to a higher AC. There is a strong dependency on the regularisation parameter. A high



(a) acoustic contrast AC [dB] (higher is better)



(b) reproduction error RE [dB] (lower is better)

 Figure 9: Comparison of the solution dependent on the Mach number and the regularisation parameter with neglected wind (red) and considered wind (blue) at $f = 600$ Hz.

regularisation parameter decreases the AC for $Ma = 0$, but it rises the solution's robustness against small errors in the input. This robustness leads to the fact that the unregularised solution performs worse in terms of the AC than the solution with the regularisation parameter $\lambda = 0.01$ and the Mach number $Ma > 0.012$. The unregularised performance undercuts the performance of the even higher regularised solution with $\lambda = 0.1$ and $Ma > 0.032$.

For the AC with considered wind, a slight, general downwards trend is visible for all regularisation parameters. This is probably due to the fact that the wind stretches and compresses the sound waves dependent on the direction of the sound wave front to the wind. Since for a given microphone not all speakers are located in the same direction, the sound waves get stretched and compressed differently. Therefore, with rising Mach numbers Ma , it is harder to cancel out all sound waves in the dark zone.

At first sight the RE in Figure 9b shows an unexpected behaviour. For neglected wind, the RE decreases with small Mach numbers

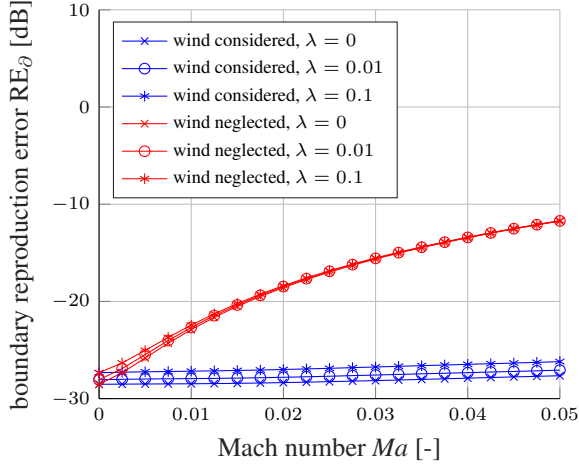


Figure 10: Comparison of the reproduction error RE_{θ} at the boundary of the bright zone for neglected and considered wind effects.

$Ma < 0.03$ and even outperforms the optimisation with considered wind in this regime. However, this is only an effect caused by the microphone setup and the definition of the RE. For example if we compute the RE, closer to the areas where the pressure is optimised (positions of the microphones), this effect vanishes, as can be seen from Figure 10. It shows the RE computed at the boundary of the bright zone (denoted by RE_{θ}). It is visible that neglecting the wind leads to an increase in the RE_{θ} , even for small Mach numbers.

Similarly to Section 3.1, the RE and also the RE_{θ} is quite resistant to changes in the regularisation parameter in the studied Mach number range. Furthermore, a slow increasing RE and RE_{θ} is visible with rising Mach numbers, which is probably due to the same reason as the decreasing AC with higher Mach numbers.

3.3 Sound Field Reproduction under Harsh Environmental Conditions

In order to show that the proposed methodology works under harsh environmental conditions, we examine a more complex setting based on simulations of 2D Euler equations.

Simulation Setup The distribution of the microphones and the speakers remains unchanged (see Figure 11). The underlying wind profile is logarithmic $(0.4673Ma \cdot c \ln((y + 2.3 \text{ m})/0.3 \text{ m}), 0)$ m/s as proposed in [14] for atmospheric boundary layers with c being the speed of sound. The wind speed corresponds to the wind speed at $y = 0$ m and it is set to 5 Bft (9.35 m/s). In addition to a nonuniform wind profile, a temperature gradient of $3^\circ\text{C}/\text{m}$ and $30^\circ\text{C}/\text{m}$ is introduced (see Figure 11) where at $y = 0$ m the speed of sound is 343 m/s. With this setup, no analytical sound field is known.

The training data for the networks is created using a high order finite difference solver of the Euler equations in 2D.⁷ The reduction

⁷See G for relevant parameters of the simulation. See [12] for time and space discretisation schemes and boundary conditions.

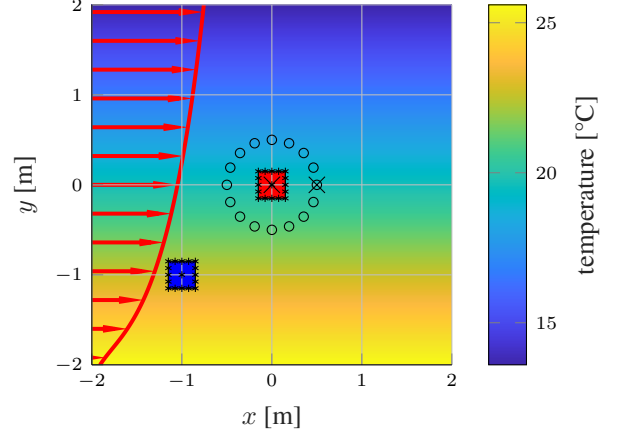


Figure 11: Geometry of the setup. The red square is the bright zone and the blue square is the dark zone. Circles are indicators for speakers, asterisks for microphones. The temperature can be read from the colour scale ($3^\circ\text{C}/\text{m}$ temperature gradient case). The logarithmic wind profile is shown where the wind speed corresponds to the wind speed at $y = 0$ m.

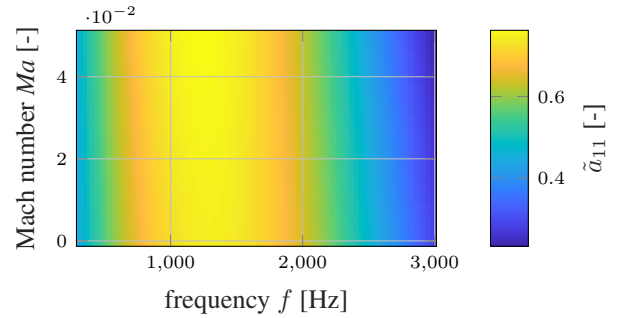


Figure 12: Amplitude modulation \tilde{a}_{11} [-] of the acoustic transfer function between the speaker and microphone indicated with a cross in Figure 11 which shows the frequency dependency of the amplitude modulation due to the source not being a point source.

from 3D to 2D was done to speed up the process of training data creation. Since there is no qualitative difference to sound propagation from 2D to 3D, this does not reduce the meaning of the showcase.⁸ Since a finite difference solver is used, the speakers cannot be modelled as point sources but rather as a source with the Gaussian function as spacial distribution. This leads to a frequency dependency of the amplitude modulation \tilde{a} of the acoustic transfer functions (see Figure 12) which can easily be learned by the neural networks.

Results Figure 13 shows the sound energy density level relative to the bright zone with considered and neglected wind and temperature ($3^\circ\text{C}/\text{m}$ gradient case) influence. It is easily visible that the consideration of both influences leads to a higher AC.

⁸In 3D the amplitude of the pressure reduces inverse proportional to the distance s to the sound source. In 2D it reduces inverse proportional to the square root of the distance \sqrt{s} to the sound source.

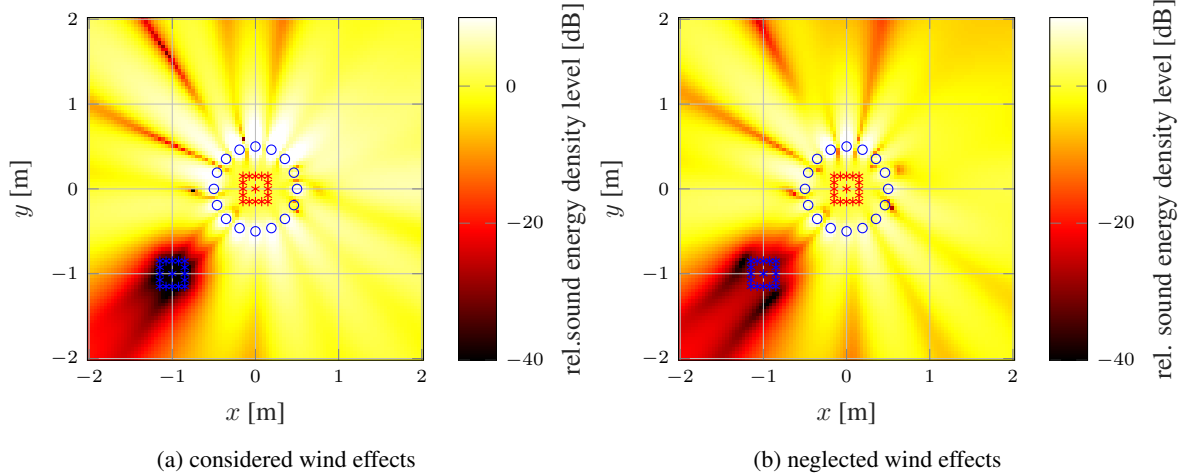


Figure 13: Comparison of the sound energy density level [dB] relative to the bright zone at frequency $f = 600$ Hz and regularisation parameter $\lambda = 0$ with considered and neglected wind effect at Mach number $Ma = 0.0275$ (5 Bft) and temperature stratification at 3°C/m gradient.

An overview of the results when neglecting or considering wind and/or the temperature gradient of 3°C/m are shown in Table 1. As in the previous cases, abstracting from wind leads to a drop of the AC by 16 dB. Also the RE is by 17 dB higher compared to the model that includes wind dynamics.

The consideration of the temperature gradient of 3°C/m seems to have a very small impact for this case since both AC and RE do not differ by more than 1 dB. It is expected that the RE is not strongly affected by the temperature gradient since the temperatures are not significantly different from the temperatures in the middle of the domain. However, the dark zone is by 3 K warmer than the bright zone which leads to an increase of 0.7% of the speed of sound. With the regularisation parameter $\lambda = 0$ the wind with the Mach number $Ma < 0.007$ already had an effect on the AC in the previous case. The influence of this effect can be bigger in real applications where the distance between the speakers and the microphones is much larger and therefore smaller temperature gradients can have a higher effect on the solution.

To show that the temperature can influence the results, a second setup with a high temperature gradient of 30°C/m is introduced. The results are displayed in Table 2 and it is visible that neglecting the temperature gradient leads to worse performance of the multi zone sound field reproduction. Interestingly, when ignoring wind, the absence of the temperature gradient in the model leads only to small additional errors in the AC (2.7 dB) and negligible differences in the RE (0.1 dB). Both setups imply that the proposed methodology works for setups where no analytical solution of the sound propagation is available.

4 Discussion

This manuscript provides a proof of concept for a new multi zone sound field reproduction approach that considers harsh environmental conditions. Our method is able to reproduce results from [6] and capable of considering several physical effects that influence sound propagation e.g. wind, temperature stratification, reflections and dispersion.

wind status	temperature gradient considered	temperature gradient neglected
wind considered	AC = 45.1 dB, RE = -33.5 dB	AC = 44.4 dB, RE = -33.9 dB
wind neglected	AC = 28.6 dB, RE = -16.4 dB	AC = 28.7 dB, RE = -16.5 dB

Table 1: Comparison of the wind profiles at $Ma = 0.0275$ (5Bft) (at $y = 0$ m) and the temperature gradient of 3°C/m on the RE and AC.

wind status	temperature gradient considered	temperature gradient neglected
wind considered	AC = 46.5 dB, RE = -33.5 dB	AC = 32.7 dB, RE = -29.6 dB
wind neglected	AC = 28.8 dB, RE = -16.5 dB	AC = 26.1 dB, RE = -16.4 dB

Table 2: Comparison of the wind profiles at $Ma = 0.0275$ (5 Bft) (at $y = 0$ m) and the temperature gradient of 30°C/m on the RE and AC.

The results show that the proposed methodology works well for setups with wind and temperature stratification. The magnitude of the physical effect correlates with the difference in quality of the solution between abstracting from wind and temperature or explicitly account for these environmental influences.

Furthermore the results show that the regularisation parameter plays an important role in the decision whether to consider physical effects or not. A stronger regularisation leads to larger costs for the control variables (speaker signal). Therefore, the optimisation procedure will tend to neglect additional physical effects, like wind.

When using simulations for the creation of the training data, the methodology can be initially computationally intensive since the nonlinear effects of wind, temperature fluctuations and other possible effects need to be simulated which leads to solving the Euler equations in 3D. Using measurements can simplify the creation of the training data. One should keep in mind that only the creation of the training data is computationally intensive. After the neural networks have been trained, they can be rapidly evaluated and used inside the optimisation problem. In this way we can instantly generate an optimised speaker signal, which is adapted to the measured wind and temperature values.

It is important to note that training neural networks to replicate nonlinear physical effects on the transfer functions can be used by all methods that are based on transfer functions.

Future studies can possibly explore studying and generalising the framework for complex geometries like rooms. Another point of interest is to test the framework in physical experiments instead of numerical experiments. The framework can also be used to serve as an initial guess for sound field reproduction with adjoint methods to decrease its computational intensity.

Declaration of competing interest

The authors declare that they have no known competing financial interests or personal relationships that could have appeared to influence the work reported in this paper.

Author Contribution Statement (CRediT)

Henry Sallandt: Conceptualisation, Methodology, Software, Investigation, Writing - Original Draft, Visualisation

Philipp Krahl: Conceptualisation, Methodology, Writing - Original Draft, Supervision, Writing - Review & Editing

Mathias Lemke: Conceptualisation, Software (CAA solver), Supervision, Writing - Review & Editing

Acknowledgement

The authors acknowledge financial support by the Deutsche Forschungsgemeinschaft (DFG) within the project LE 3888/2. Philipp Krahl gratefully acknowledges the support of the Deutsche Forschungsgemeinschaft (DFG) as part of GRK2433 DAEDALUS.

References

- [1] Bailly, C., Juvé, D., 2000. Numerical Solution of Acoustic Propagation Problems Using Linearized Euler Equations. *AIAA Journal* 38, 22–29. doi:<https://doi.org/10.2514/2.949>.
- [2] Bianco, M.J., Gerstoft, P., Traer, J., Ozanich, E., Roch, M.A., Gannot, S., Deledalle, C.A., 2019. Machine learning in acoustics: Theory and applications. *The Journal of the Acoustical Society of America* 146 5, 3590. doi:<https://dx.doi.org/10.1121/1.5133944>.
- [3] Boone, M.M., Verheijen, E.N.G., van Tol, P.F., 1995. Spatial Sound-Field Reproduction by Wave-Field Synthesis. *Journal of the Audio Engineering Society* 43, 1003 EP – 1012. URL: <https://www.aes.org/e-lib/browse.cfm?elib=7920>.
- [4] Choi, J.W., Kim, Y.H., 2002. Generation of an acoustically bright zone with an illuminated region using multiple sources. *The Journal of the Acoustical Society of America* 111, 1695–700. doi:<https://doi.org/10.1121/1.1456926>.
- [5] Ciaburro, G., Iannace, G., 2021. Acoustic Characterization of Rooms Using Reverberation Time Estimation Based on Supervised Learning Algorithm. *Applied Sciences* 11. doi:<https://doi.org/10.3390/app11041661>.
- [6] Du, B., Zeng, X., Vorländer, M., 2021. Multizone Sound Field Reproduction Based on Equivalent Source Method. *Acoustics Australia* 49, 317–329. doi:<https://doi.org/10.1007/s40857-021-00228-3>.
- [7] Gerzon, M.A., 1975. The Design of Precisely Coincident Microphone Arrays for Stereo and Surround Sound, in: *Audio Engineering Society Convention* 50, pp. L–20. URL: <http://www.aes.org/e-lib/browse.cfm?elib=2466>.
- [8] Hansen, P.C., 2021. regtools. URL: <https://www.mathworks.com/matlabcentral/fileexchange/52-regtools>. retrieved 2021-07-28.
- [9] Heuchel, F., Caviedes Nozal, D., Agerkvist, F.T., 2018. Sound field control for reduction of noise from outdoor concerts, in: *Audio Engineering Society Convention* 145, Audio Engineering Society.
- [10] Lange, H., Brunton, S.L., Kutz, J.N., 2020. From Fourier to Koopman: Spectral Methods for Long-term Time Series Prediction. CoRR abs/2004.00574. URL: <https://arxiv.org/abs/2004.00574>. arXiv: 2004.00574.
- [11] Lei, Q., Chen, H., Hou, J., Chen, L., Dai, L., 2019. Deep Neural Network Based Regression Approach for Acoustic Echo Cancellation, in: *Proceedings of the 2019 4th International Conference on Multimedia Systems and Signal Processing, Association for Computing Machinery, New York, NY, USA*. pp. 94–98. doi:<https://doi.org/10.1145/3330393.3330399>. event-place: Guangzhou, China.
- [12] Lemke, M., 2015. Adjoint based data assimilation in compressible flows with application to pressure determination from PIV data. Doctoral Thesis. Technische Universität Berlin. Berlin. URL: <http://dx.doi.org/10.14279/depositonce-4909>,

doi:10.14279/depositonce-4909. publication Title: Technische Universität Berlin.

- [13] Lemke, M., Straube, F., Schultz, F., Sesterhenn, J., Weinzierl, S., 2017. Adjoint-Based Time Domain Sound Reinforcement, in: Audio Engineering Society Conference: 2017 AES International Conference on Sound Reinforcement – Open Air Venues, p. P2.2. URL: <http://www.aes.org/e-lib/browse.cfm?elib=19178>.
- [14] Richards, P., Hoxey, R., 1993. Appropriate boundary conditions for computational wind engineering models using the k- ϵ turbulence model. Proceedings of the 1st International on Computational Wind Engineering 46-47, 145–153. doi:<https://doi.org/10.1016/j.jweia.2010.12.008>.
- [15] Shin, M., Fazi, F.M., Nelson, P.A., Hirono, F.C., 2014. Controlled sound field with a dual layer loudspeaker array. Journal of Sound and Vibration 333, 3794–3817. URL: https://eprints.soton.ac.uk/365408/1/Shin_et_al_Controlled%2520sound%2520field%2520with%2520a%2520dual%2520layer%2520loudspeaker%2520array_EPRINT.pdf.
- [16] Stein, L., Straube, F., Sesterhenn, J., Weinzierl, S., Lemke, M., 2019a. Adjoint-based optimization of sound reinforcement including non-uniform flow. The Journal of the Acoustical Society of America 146, 1774–1785. doi:<https://doi.org/10.1121/1.5126516>.
- [17] Stein, L., Straube, F., Sesterhenn, J., Weinzierl, S., Lemke, M., 2019b. Adjoint-based sound reinforcement in the time domain, in: Proceedings of the 23rd International Congress on Acoustics.
- [18] Tikhonov, A., Goncharky, A., Stepanov, V., Yagola, A., 1990. Numerical Methods for the Solution of Ill-Posed Problems. Springer, Moscow.
- [19] Y. Long, Y. Li, S. Wei, Q. Zhang, C. Yang, 2019. Large-Scale Semi-Supervised Training in Deep Learning Acoustic Model for ASR. IEEE Access 7, 133615–133627. doi:<https://doi.org/10.1109/ACCESS.2019.2940961>.
- [20] Zotter, F., Frank, M., 2019. Ambisonics. Springer Topics in Signal Processing, Springer, Cham. URL: <https://library.oapen.org/handle/20.500.12657/23095>.

A Discontinuity in Phase Angle

For a 2π -periodic function $f(x) = y$ it holds $f(x) = f(2\pi n + x)$ with $n \in \mathbb{Z}$. Therefore the inverse function $f^{-1}(y) = x$ only returns values in the interval $[-\pi, \pi]$. This leads to a discontinuity when x surpasses the previously stated interval $[-\pi, \pi]$ which is displayed in Figure 14.

The first option would be to detect the discontinuities by looking at the finite difference quotient and then stitching the discontinuities together to get the original function. This leads to the problem that the original function is not bounded and also the stitching process can be complicated when having only few sample points of the function.

The second option is to plug the values into a function that leads to an injective but continuous mapping and train the neural network on the result(s). After evaluating the neural networks the inverse mapping needs to be evaluated to get the original x . The chosen function leads to two results v_1 and v_2 that need to be learned:

$$v_1 = \cos(x) \quad (20)$$

$$v_2 = \sin(x) \quad (21)$$

The inverse mapping is the four quadrant inverse tangens $x = \text{atan2}(v_2, v_1)$.

B Derivation of Green’s Function of the 3D Wave Equation with Uniform Background Flow

We now seek Green’s Function $\mathcal{G}(x, y, z, t)$ of the d’Alembert operator (hence 3D wave equation) in a free field with a uniform subsonic mean flow of the form $(u_0, 0, 0)$. This is done similar to [1], but in 3D. The wave equation of the system is the following:

$$\frac{d^2 \mathcal{G}}{dt^2} - c^2 \nabla^2 \mathcal{G} = \delta(x, y, z) \exp(-i\omega t), \quad (22)$$

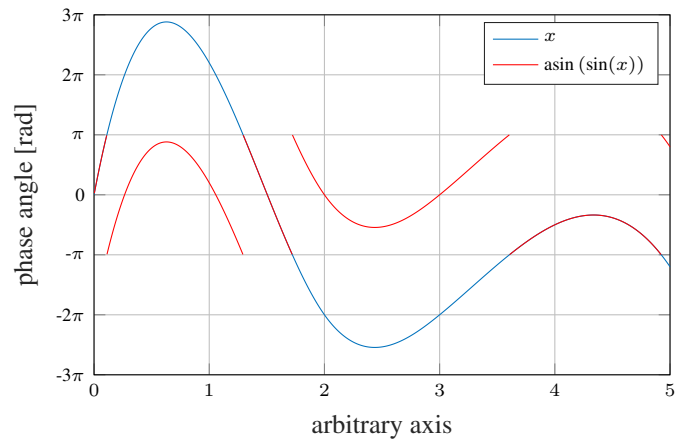


Figure 14: Discontinuity problem: The periodicity of the $\sin(x)$ function leads to a discontinuity for $\text{asin}(\sin(x))$ if x surpasses $[-\pi, \pi]$.

where $\frac{d}{dt} = \frac{\partial}{\partial t} + u_0 \frac{\partial}{\partial x}$. With the introduction of a coordinate system moving with the mean flow $\tilde{t} = t$, $\tilde{x} = x - u_0 t$, $\tilde{y} = y$, $\tilde{z} = z$ the wave equation becomes

$$\frac{\partial^2 \tilde{\mathcal{G}}}{\partial \tilde{t}^2} - c^2 \tilde{\nabla}^2 \tilde{\mathcal{G}} = \delta(\tilde{x} + u_0 \tilde{t}, \tilde{y}, \tilde{z}) \exp(-i\omega \tilde{t}), \quad (23)$$

with $\tilde{\mathcal{G}}(\tilde{x}, \tilde{y}, \tilde{z}, \tilde{t}) = \mathcal{G}(x, y, z, t)$ and δ being the δ distribution. Green's function can be calculated in the primitive variables as:

$$\mathcal{G}(x, y, z, t) = \frac{\exp(-i\omega t)}{4\pi} \int \frac{\exp(i\omega \tau) \theta(\tau)}{\sqrt{(x - u_0 \tau)^2 + y^2 + z^2}} \cdot \delta\left(\tau - \sqrt{\frac{(x - u_0 \tau)^2 + y^2 + z^2}{c^2}}\right) d\tau. \quad (24)$$

Here, θ is the Heaviside function. The sampling property of the delta distribution can be used to solve the integral by finding the delta distribution's argument root.

$$0 = \tau - \sqrt{\frac{(x - Ma c \tau)^2 + y^2 + z^2}{c^2}} \quad (25)$$

The root of the argument can be calculated as

$$\tau^{1/2} = -\frac{(xMa \pm \sqrt{x^2 + (1 - Ma^2)(y^2 + z^2)})}{(1 - Ma^2)c}. \quad (26)$$

Both values τ^1 and τ^2 need to be checked if they are bigger than 0 because of the Heaviside function. Every positive value is plugged into the integral's argument in Equation (24) and added together to get Green's function. The source term of the speaker is of the form $q = \hat{q}(x, y, z) \exp(-i\omega t)$. Therefore the space convolution product of \hat{q} and \mathcal{G} gives the pressure distribution.

C Iteration Process of Calculating the Wave Number Modulation Factor

The goal of this calculation is that the phase modulation is constant with respect to the frequency (or more general: the mean derivative with respect to the frequency is minimised). The wind leads to a contraction or an extension of the sound waves. Since in this application a relatively small Mach number $Ma \ll 1$ is examined the initial wave number modulation of $\tilde{k}^{l=0} = 1$ can be assumed. The resulting phase angle can be calculated and if the wave number modulation was correctly assumed this would result in a constant phase modulation with respect to the frequency.

Figure 2 shows the phase modulation for the first 3 iterations. Figure 16b visualises the respective wavenumber modulation factors for the first 3 iterations. It is visible that for low Mach numbers the assumption of a wave number modulation $\tilde{k} = 1$ is quite accurate. With higher Mach numbers the contraction or extension of the sound waves becomes stronger. To get the correct wave number modulation \tilde{k} the absolute value of the partial derivative of the wrong corrected phase angle $\tilde{\varphi}$ needs to be minimised. This can be achieved with a gradient descent method.

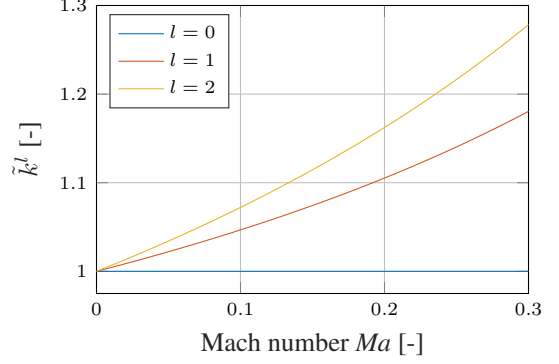
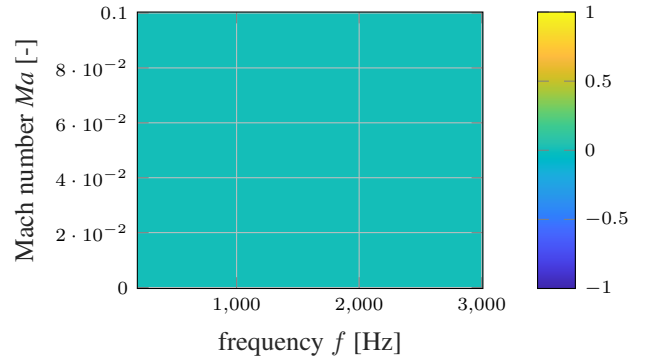


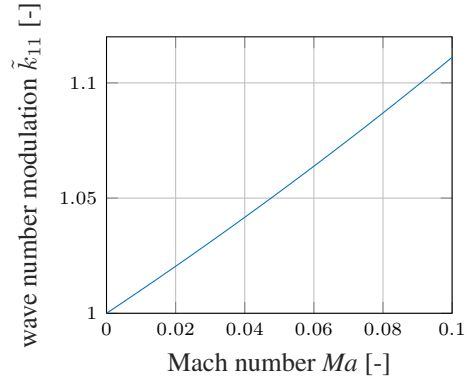
Figure 15: evolution of the wave number correction factor \tilde{k}^l / π

D Other Functions to be Learned by the Neural Networks

The functions are displayed in Figure 16.



(a) phase modulation $\tilde{\varphi}_{11} [-]$



(b) wave number modulation $\tilde{k}_{11} [-]$

Figure 16: Two remaining of the three functions to be learned for microphone 1 and speaker 1 (see Figure 6 for location).

E Resonance of the Microphone Array

To further examine the resonance in the bright zone another setup with a bigger square side length of 0.4 m (square side length of the

original setup is 0.3 m) is considered and visualised in Figure 17. The training data is created using Green’s function of the wave equation in 3D.

Figure 18 shows the RE over the previously considered frequency interval [200,1000] Hz. The resonance that can be seen in Figure 5a and occurs at the frequency 810 Hz for the original setup occurs in the examined setup at 600 Hz. This resonance can again be inhibited by introducing the microphone in the middle of the microphone array. A second resonance is visible in Figure 19 and occurs at approx. 940 Hz. For the original setup this resonance was not inside the considered frequency interval. The placement of the microphone in the middle of the bright zone does not lead to the inhibition of the second resonance since the antinodes of this resonance are not located in the middle of the square.

F Effect of Noise on the Solution

To get a feeling of the effects of noise on the solution an examination of the AC and the RE dependent on the signal to noise ratio SNR (in dB) and variance σ^2 of the noise is done. The SNR is distributed with a normal distribution with different mean values and different variances.

The noise gets added to the acoustic transfer functions in the following way:

$$g_{\text{noise}} = g + 10^{-\frac{\text{SNR}}{10 \text{ dB}}} \cdot |g| \exp(i\varphi) \quad (27)$$

The phase angle φ is randomly and uniformly distributed in the interval $[-\pi, \pi]$. For the uniformly distributed case the variance is set to 0 and the noise term gets scaled by an additional randomly and uniformly distributed scalar in the interval $[0, 1]$. The regularisation parameter is chosen according to the L-curve method using [8].

The results are shown in Figure 21 for the AC and in Figure 20 for the RE. Since the RE is quite resistant to changes in the regularisation parameter, the effect of the noise on the RE can be assessed. It is visible that a SNR of 30 dB only leads to minor changes in the RE where a smaller SNR of 10 dB leads to

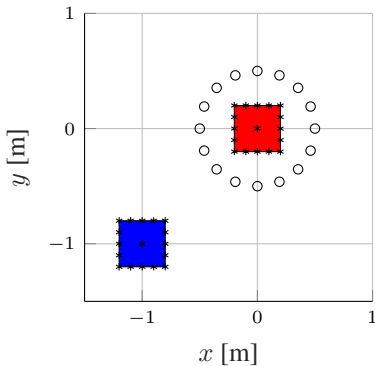


Figure 17: Simulation setup of the additional setup. The square side length is 0.4 m instead of 0.3 m. The red square is the bright zone and the blue square is the dark zone. Circles (o) are indicators for speakers, asterisks (*) for microphones. Again the setups with a microphone in the middle of the squares and without are compared.

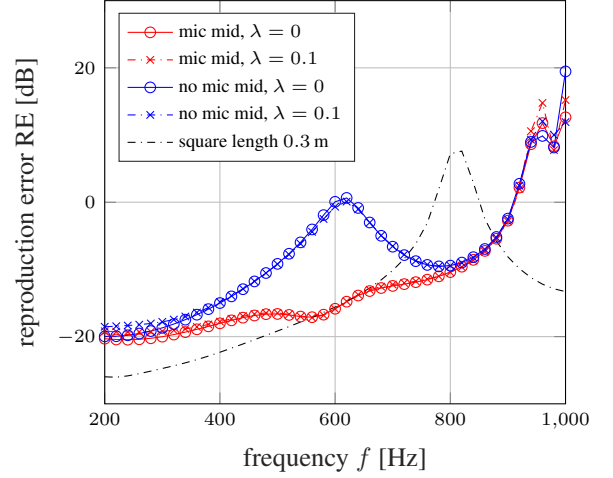


Figure 18: Comparison of results with a microphone in the middle and without a microphone in the middle. The wind speed is set to zero. For a better comparison the original setup’s solution without microphone in the middle is also shown.

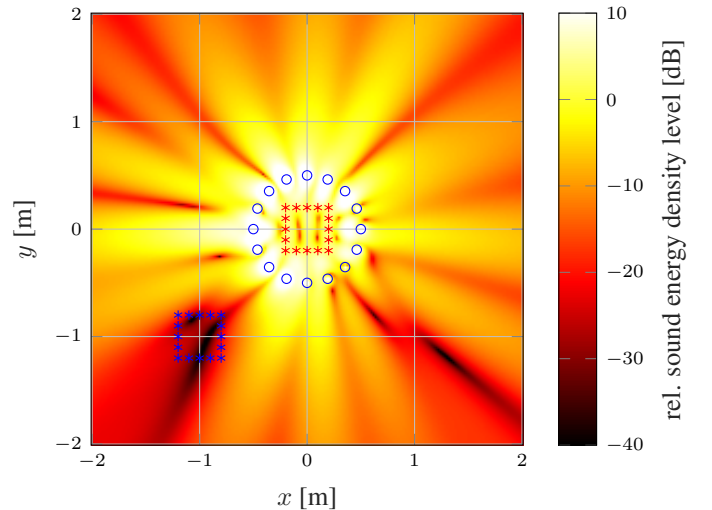


Figure 19: The unregularised solution without wind at $f = 940$ Hz is visualised to show the second resonance.

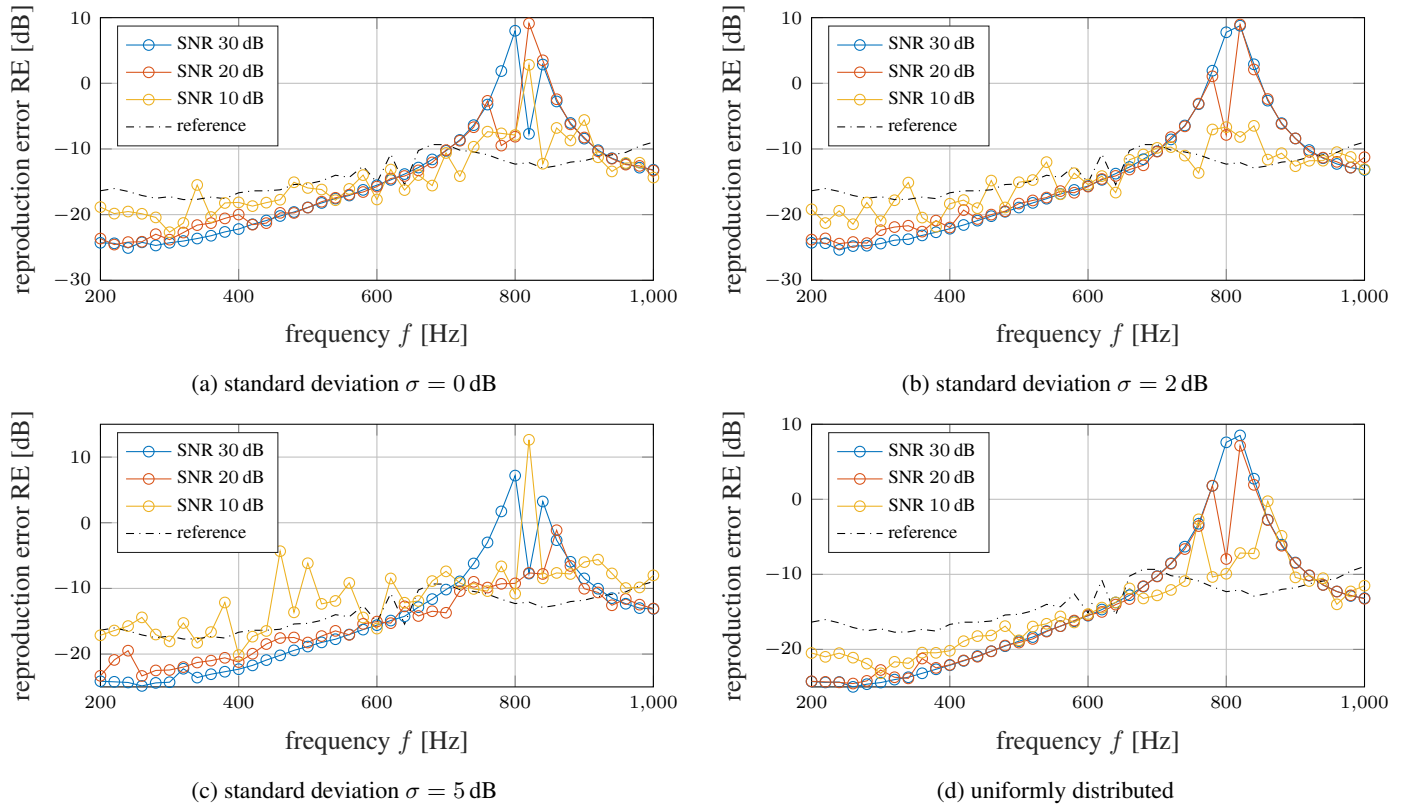


Figure 20: RE dependent on the signal to noise ratio SNR, regularisation according to L-curve method

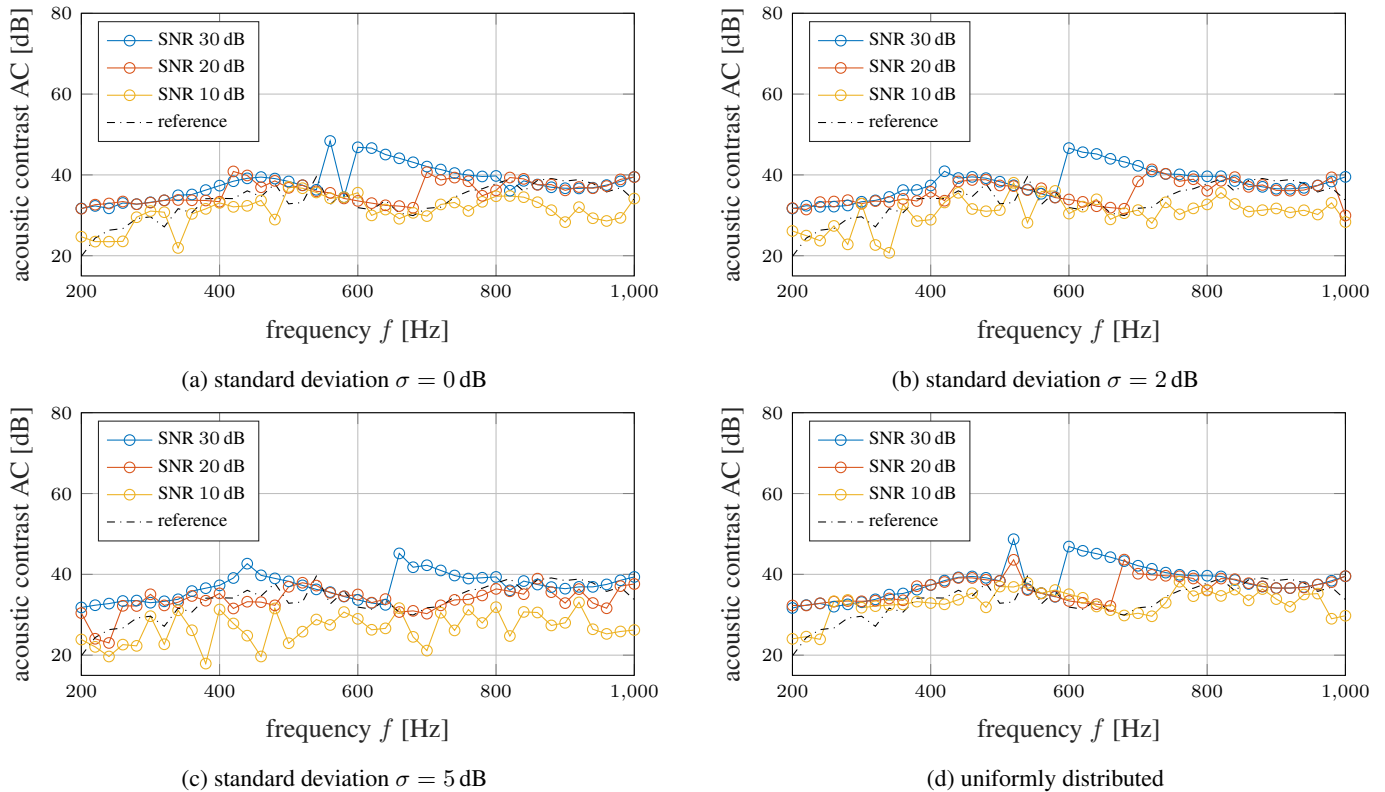


Figure 21: Dependence of AC on the signal to noise ratio SNR with regularisation according to L-curve method as in [6].

bigger changes and an approximation of the RE to the reference values.

The AC however shows that even with a big SNR of 30 dB big changes in the AC are notable. The regularisation parameter is chosen according to the L-curve method. In Figure 4a it is visible, that the regularisation parameter has a big influence on the AC. This leads to the possibility that changes in the AC can also be induced by the noise's impact on the L-curve method or fluctuations of the L-curve method itself.

G Parameters for the 2D Finite Difference Euler Equation Simulation

The spatial and temporal discretisation schemes and boundary conditions are described in [12].

The simulation is done in a $8\text{m} \times 8\text{m}$ free field domain (non-reflecting boundary conditions) discretised with 500 uniformly spaced points with the grid size h in x and y direction. The domain size is chosen in a way to prevent errors in the non-reflecting boundary conditions at the boundary of the domain to influence the results.

The time step $\Delta t = 1/(48\text{ kHz})$ is chosen to match the common sampling frequency of 48 kHz. We use 800 time steps in total, where the last 100 time steps are treated as the steady state solution.

A speed of sound $c = 343\text{ m/s}$ is realised at $y = 0\text{ m}$. The adiabatic index is set to $\gamma = 1.4$ and the ambient values are as following: The ambient pressure $p_\infty = 101325\text{ Pa}$, the specific gas constant of air $R_s = 287.058\text{ J/(kgK)}$ and the temperature $T = 19.597\text{ }^\circ\text{C} + |\nabla T|y$. The horizontal component of the wind profile is introduced as $u_x = 0.4673Ma \cdot c \cdot \ln((y + 2.3\text{ m})/0.3\text{ m})$. Scaled to the wind speed of 5 Bft(9.35 m/s at $y = 0\text{ m}$ this leads to a maximum wind speed of 11.63 m/s at $y = 2\text{ m}$. Below of $y = -2\text{ m}$ the component is set to $u_x = 0\text{ m/s}$. In the vertical direction the wind is set to $u_y = 0$. The horizontal wind component is smoothed around the kink at $y = -2.3\text{ m}$. This is done using a circle with radius 0.4.